⑫

David Taylor Research Center
Bethesda, MD 20084–5000

Chaos Displayed by Solutions of a Forced Pendulum Equation with a Fifth–Order Polynomial for the Damping Terms

by
Hans J. Lugt
Michael L. Brabanski

DTIC
S ELECTE D
NOV 3 0 1990
E

AD–A229 496

DTRC–90/031   Chaos Displayed by Solutions of a Forced Pendulum Equation with a Fifth–Order Polynomial for the Damping Terms

MAJOR DTRC TECHNICAL COMPONENTS

CODE 011 DIRECTOR OF TECHNOLOGY, PLANS AND ASSESSMENT

12 SHIP SYSTEMS INTEGRATION DEPARTMENT

14 SHIP ELECTROMAGNETIC SIGNATURES DEPARTMENT

15 SHIP HYDROMECHANICS DEPARTMENT

16 AVIATION DEPARTMENT

17 SHIP STRUCTURES AND PROTECTION DEPARTMENT

18 COMPUTATION, MATHEMATICS & LOGISTICS DEPARTMENT

19 SHIP ACOUSTICS DEPARTMENT

27 PROPULSION AND AUXILIARY SYSTEMS DEPARTMENT

28 SHIP MATERIALS ENGINEERING DEPARTMENT

DTRC ISSUES THREE TYPES OF REPORTS:

1. **DTRC reports, a formal series,** contain information of permanent technical value. They carry a consecutive numerical identification regardless of their classification or the originating department.

2. **Departmental reports, a semiformal series,** contain information of a preliminary, temporary, or proprietary nature or of limited interest or significance. They carry a departmental alphanumerical identification.

3. **Technical memoranda, an informal series,** contain technical documentation of limited use and interest. They are primarily working papers intended for internal use. They carry an identifying number which indicates their type and the numerical code of the originating department. Any distribution outside DTRC must be approved by the head of the originating department on a case-by-case basis.

REPORT DOCUMENTATION PAGE

REPORT SECURITY CLASSIFICATION	1b. RESTRICTIVE MARKINGS

SECURITY CLASSIFICATION AUTHORITY UNCLASSIFIED	3. DISTRIBUTION/AVAILABILITY OF REPORT
DECLASSIFICATION/DOWNGRADING SCHEDULE	Approved for public release; distribution is unlimited.

PERFORMING ORGANIZATION REPORT NUMBER(S) DTRC–90/031	5. MONITORING ORGANIZATION REPORT NUMBER(S)

NAME OF PERFORMING ORGANIZATION David Taylor Research Center	6b. OFFICE SYMBOL (If applicable) Code 1802	7a. NAME OF MONITORING ORGANIZATION

ADDRESS (City, State, and ZIP Code) Bethesda, Maryland 20084–5000	7b. ADDRESS (City, State, and ZIP Code)

NAME OF FUNDING/SPONSORING ORGANIZATION	8b. OFFICE SYMBOL (If applicable)	9. PROCUREMENT INSTRUMENT IDENTIFICATION NUMBER

ADDRESS (City, State, and ZIP Code)	10. SOURCE OF FUNDING NUMBERS			
	PROGRAM ELEMENT NO. 61152N	PROJECT NO.	TASK NO.	WORK UNIT ACCESSION NO.

TITLE (Include Security Classification)
Chaos Displayed by Solutions of a Forced Pendulum Equation with a Fifth–Order Polynomial for the Damping Terms

PERSONAL AUTHOR(S)
Lugt, Hans J. and Brabanski, Michael L.

TYPE OF REPORT Final	13b. TIME COVERED FROM_____ TO_____	14. DATE OF REPORT (YEAR, MONTH, DAY) 1990, November	15. PAGE COUNT 36

SUPPLEMENTARY NOTATION

COSATI CODES			18. SUBJECT TERMS (Continue on reverse if necessary and identify by block number)
FIELD	GROUP	SUB–GROUP	Chaos, forced pendulum equation, autorotation, self–sustained oscillation

ABSTRACT (Continue on reverse if necessary and identify by block number)

Solutions of a forced pendulum equation of one degree–of–freedom with nonlinear damping terms have been studied for chaotic and dissipative behavior. This equation can simulate phenomena in which vortex shedding from oscillating and rotating bodies is involved. The characteristic properties of this equation, that is, its singular points, attractors, separatrices, etc. are investigated and related to their physical meaning. A novel attractor is found that represents simultaneously autorotation and self–sustained oscillation. Chaotic behavior is studied with Poincaré maps and power spectra. Strange attractors exist which are insensitive to various pendulum coefficients.

DISTRIBUTION/AVAILABILITY OF ABSTRACT ☐ UNCLASSIFIED/UNLIMITED ☒ SAME AS RPT ☐ DTIC USERS	21. ABSTRACT SECURITY CLASSIFICATION UNCLASSIFIED
NAME OF RESPONSIBLE INDIVIDUAL Hans J. Lugt	22b. TELEPHONE (Include Area Code) (301) 227–1925	22c. OFFICE SYMBOL Code 1802

FORM 1473, JUN 86   Previous editions are obsolete

CONTENTS

FIGURES

ABSTRACT

Solutions of a forced pendulum equation of one degree-of-freedom with nonlinear damping terms have been studied for chaotic and dissipative behavior. This equation can simulate phenomena in which vortex shedding from oscillating and rotating bodies is involved. The characteristic properties of this equation, that is, its singular points, attractors, separatrices, etc. are investigated and related to their physical meaning. A novel attractor is found that represents simultaneously autorotation and self-sustained oscillation. Chaotic behavior is studied with Poincaré maps and power spectra. Strange attractors exist which are insensitive to various pendulum coefficients.

ADMINISTRATIVE INFORMATION

BACKGROUND

The relative simplicity of the pendulum equation, its easy integration on today's computers, and its physical lucidity have made the study of this equation often a paradigm for investigating nonlinear processes in which chaotic and dissipative behavior is involved. Books by Thompson and Stewart,[1] Moon,[2] and Schuster[3] may be mentioned. In addition to this more educational aspect, the pendulum equation has been proven a reasonably accurate model for a number of complicated physical phenomena.

Of Navy interest are pendulum-type equations that model the rolling motion of ships.[4,5] This motion can exhibit chaotic behavior.[6]

Another example of Navy interest is the usefulness of an extended pendulum equation to describe rotating and oscillating objects in a fluid, a problem whose solution otherwise would require the numerical integration of a set of nonlinear partial differential equations. This case will be studied in this report in more detail.

The involvement of the simple pendulum equation

$$\ddot{x} + D \sin x = 0 \tag{1}$$

in the movement of bodies in fluid flows can be shown directly in the case of an infinitely long plate rotating or oscillating in a potential flow with the axis free to move.[7] The displacement angle is x and the angular velocity is $\dot{x}$, with the dot indicating differentiation with respect to time. D is the square root of the natural frequency for small oscillations with the moment of inertia

normalized to unity. Two initial conditions must be prescribed to make the solution unique. For a viscous fluid the senior author related in two papers[8,9] vortex shedding from oscillating and rotating bodies with the axis fixed in a parallel flow to a nonlinear model of one degree-of-freedom. It was argued that, at least qualitatively, a fifth-order polynomial for the damping term in the pendulum equation is necessary to simulate self-sustained (or self-excited) oscillation and rotation with a stable rest state

$$\ddot{x} + A\dot{x} + B\dot{x}^3 + C\dot{x}^5 + D \sin x = 0 \ , \tag{2}$$

where the coefficients A through D are constants, and at least one of the coefficients A, B, and C must be negative. For a bounded solution, the highest damping term is assumed to be positive, that is, $C > 0$; and $B > 0$ only if $C = 0$. If the lowest damping term is positive, the state at rest is stable; if it is negative, the state at rest is unstable. Thus, a qualitative difference between a third-order and a fifth-order polynomial for damping occurs only for the combination $A > 0$, $B < 0$, $C > 0$ for the fifth-order and $A < 0$, $B > 0$ for the third-order damping.

Various simplified forms of Eq. (2) have been studied in the literature. The case closest to Eq. (2) with $C = 0$ and with an additional constant K_0 (which will be introduced below) is known as the *Froude pendulum*.[2,10]

The need for a fifth-order damping polynomial can be inferred from the fifth-order curve for the torque T of a rotating body in a constant parallel stream as a function of the angular velocity $\Omega = \dot{x}$ (in the case of oscillation or time-dependent rotation, the average torque T as a function of frequency), which was named the *Riabouchinsky* curve[8] (Fig. 1). This fundamental curve was verified experimentally and numerically for the Lanchester propeller, the autorotating plate, galloping, and vortex-induced vibration, and is also applicable to other vortex-related phenomena like the autorotation-in-roll of aircraft and the rolling motion of ships.[8]

The meaning of the curve in Fig. 1a may be explained with reference to a rotating propeller in a parallel flow in the following way: A motor drives a propeller with constant angular velocity Ω. The torque T necessary to drive the propeller is measured as a function of Ω. When Ω is either quite small or quite large, a (positive) torque is necessary. Between these values an Ω-range exists in which the torque is negative and has a braking effect. This negative value indicates a negative damping of the flow which is due to vortex shedding. If the torque of the motor is removed, the propeller increases its angular velocity until $T = 0$. This is the state of autorotation (point A in Fig. 1). The other point at which $T = 0$ is unstable (point I in Fig. 1). If point I coincides with the origin, a third-order curve suffices to demonstrate the existence of A (Fig. 1b). For self-sustained oscillation, average values of T must be used, and Ω must be replaced by the frequency of the oscillation. It is also possible that Fig. 1 represents part oscillation and part rotation as will be demonstrated in the section on chaotic behavior.

For forced oscillation and rotation, Eq. (2) must be augmented to

$$\ddot{x} + A\dot{x} + B\dot{x}^3 + C\dot{x}^5 + D \sin x = K_0 + K \sin(\omega^* t + \alpha) \ , \tag{3}$$

2

with K, ω^*, and α the amplitude, frequency, and phase angle of the forcing term, respectively. K_0 is a constant forcing term (that is, a constant torque).

Equation (3) was solved by a Runge-Kutta method with a computer program which was available as DEPAC from Sandia Laboratories. This program provided also an accuracy check that consists of the sum of relative and absolute tolerances. It is recognized that solutions of a finite-difference scheme deviate ultimately from the solutions of the original differential equations. For non-chaotic motions sufficient accuracy was obtained to ensure the validity of the curves presented as solutions of the differential equations. For chaotic motions the trajectories become unpredictable for long integration times. However, the strength of the attractors appears to overcome this deficiency, and strange attractors are found which are insensitive to the accuracy of the Runge-Kutta method for variations in the tolerance of an order of magnitude.

It is the purpose of this report to present the characteristic parameters and singular points in phase space for the two modes of oscillation and rotation and to demonstrate the chaotic behavior for various parameters with Poincaré maps and power spectra.

NON-CHAOTIC BEHAVIOR

Equations (1) and (2) do not contain a forcing term and therefore chaotic b⁻havior cannot be expected.[1]

The well-known characteristics of the simple pendulum equation (1) and the local linear behavior of the system with a damping term may serve as guides for the systematic exploration of the properties of the extended pendulum equation (2).

In the non-dissipative system, Eq. (1), the two modes of oscillation and rotation occupy in phase space $(\dot{x}, x)$ areas that are divided by a curve called a *separatrix* (Fig. 2). At $x_0 = 0$ with $D = 1$, rotation occurs for $|\dot{x}_0| > 2$ and oscillation for $|\dot{x}_0| < 2$.

The types of singular point for the linearized version of Eq. (2) can be identified easily and are discussed in elementary textbooks. In Fig. 2 two types are observed: The points $(x_0 = 0, 2\pi, etc., \dot{x}_0 = 0)$ are center points, and the points $(x_0 = \pi, 3\pi, etc., \dot{x}_0 = 0)$ are saddle points. Fixed points in Figs. 3 and 4 are spiral points.

In a dissipating system damping terms are responsible for a transient period, and trajectories lead asymptotically to an attractor, either to a fixed point or to a limit cycle. The limit cycle for the oscillating mode is a closed curve, whereas the limit cycle for rotation is a sinusoidal curve, called in Ref. 9 an *open limit cycle*. Now the separatrix does not necessarily divide the areas of the oscillating and rotating modes but divides two *basins of attraction* in which trajectories lead to different attractors.

There are two types of separatrices in the dissipative system described by Eq. (2) with all constants nonzero and $A > 0$. The first type is a sinusoidal

3

curve indicating physically the autorotation shown in Fig. 3 with $A = 0.2$, $B = -0.12$. $C = 0.01$, $D = 0.2$. However, this state is unstable. Trajectories (dotted lines) with an initial velocity $|\dot{x}|$ larger than the velocity given by the separatrix lead over a transient period to the open limit cycle (which is autorotation). Trajectories in the other basin of attraction end in a fixed point after a transient period of rotation and oscillation. Among the latter trajectories are those emanating from or ending at a saddle point. Such a trajectory is called by Thompson and Stewart[1] an *outstructure* (dashed lines). The outstructures divide the region inside the separatrices into two basins of attraction for positive and negative initial rotations. These two regions wrap around the fixed points as common attractors in ever diminishing spiral bands.

A separatrix, then, divides regions with two physically different kinds of attractors, that is, self-sustained oscillation and autorotation. Outstructures, on the other hand, although basin boundaries too, separate regions with a common attractor.

The second type of separatrix is an oval curve, indicating physically unstable oscillation. In the example shown in Fig. 4 the constants are the same as in Fig. 3 except that here $D = 2$. Trajectories outside the oval are attracted to the open limit cycle of *autorotation,* whereas the trajectories inside the oval end in a fixed point. Now the outstructures lie outside the separatrix. The regions of attraction for positive and negative initial rotations wrap around the separatrix in ever decreasing spiral bands (red and green bands, respectively, in Fig. 4).

These two types of separatrices, displayed in Figs. 3 and 4 for $D = 0.2$ and 2, respectively, merge in a limiting situation $D = D_c$, with two approximations $D = 0.80$ and $D = 0.81$ shown in Fig. 5. The separatrix here represents unstable states of both oscillation and rotation and is reminiscent of the separatrix of the conservative system in Fig. 2.

The separatrices correspond in Fig. 1a to point I, while the limit cycles correspond to point A and the fixed point to the origin of the graph.

For the case of an unstable state at rest, that is, $A < 0$, C can be put to zero without loss of generality for a qualitative discussion (Fig. 1b). Then, a closed or open limit cycle exists depending on the asymptotic state of oscillation or rotation (Figs. 6 and 7) without a separatrix. However, outstructures do exist with a saddle point. From here, one branch goes into the oval limit cycle (Fig. 6) and the other branch, coming from infinity, ends in the saddle point. The spiral point is now a repellor. Fig. 7 shows the same situation for an open limit cycle. The basins of attraction, divided by outstructures, are marked in red and green.

Here again, there is a limiting situation between the two examples, Figs. 6 and 7, as displayed in Fig. 8, which appears to contain a novel feature: Closed and open limit cycles collapse to one single braid-type curve! This attractor represents both autorotation and self-sustained oscillation, and the choice between them depends on the approach to this unusual attractor: Trajectories inside the oval are drawn to the attractor in the oscillatory mode, trajectories outside in the rotatory mode.

4

The essential qualitative difference between the third-order and the fifth-order polynomial damping terms lies in the sign of A. The change from positive to negative A represents a typical Hopf bifurcation[2], that is, the transition from a fixed-point attractor to a limit-cycle attractor. It may be pointed out that the limit cycle in this Hopf bifurcation can be both closed and open.

The presence of the constant forcing term K_0 (which represents a constant torque) does not cause chaotic motion. Increasing the value of K_0 diminishes and finally eliminates the oscillating mode, and the rotating mode prevails. Solutions of Eq. (3), with $K \sin(\omega^* t + \alpha)$ present, can display chaos. They will be discussed for some typical parameter values in the next section.

CHAOTIC BEHAVIOR

Interaction between self-excited and forced periodic motion, described by Eq. (3), can exhibit chaotic behavior. The concept of chaos is complex and difficult to define; to quote Hao:[11] "There is no generally accepted definition of chaos." Here it may be loosely defined according to Moon[2] as a "deterministic system whose time history has a *sensitive dependence on initial conditions*" and by certain criteria met in a Poincaré map and in a power spectrum.

Studies of special cases of Eq. (3) with regard to chaotic behavior abound in the literature.[2] A few examples are the papers by Pezeshki and Dowell[12] on the Duffing equation, by Gwinn and Westervelt[13] on intermittency, and by Grebogi et al.[14] on smooth and fractal basin boundaries.

In this report the patterns of strange attractors are studied for selected values of the coefficients in Eq. (3). The following coefficients were kept unchanged for all cases studied: $K_0 = 0$, $\omega^* = 1$, $\alpha = 0$ with the initial conditions $x_0 = \dot{x}_0 = 0$.

Chaotic behavior in pure oscillation was observed for $A = -0.2$, $B = 0.01$, $C = 0$, $D = 2$. and $K = 10$, displayed in Fig. 9. This case may be compared with that of Fig. 7 for $K = 0$, in which the fixed point is a repellor and the attractor an open limit cycle, that is, autorotation. The force term prevents rotation now and generates a strange attractor in the oscillatory mode seen in Fig. 10.

Figure 10 shows a Poincaré map with typical folding characteristics known from similar situations.[2] The number of points, plotted after each $\Delta t = \pi/4$, is 500.

The corresponding power spectrum is shown in Fig. 11. If the Fourier transform $\tilde{x}(\omega)$ of the function $x(t)$ is defined by

$$\tilde{x}(\omega) = \lim_{t \to \infty} \int_0^t x(t') e^{i\omega t'} dt' , \tag{4}$$

the power spectrum is

$$P(\omega) = |\tilde{x}(\omega)|^2 \ . \tag{5}$$

In Fig. 11 the function $20 \log_{10}P$ in units of decibles is plotted against the frequency ω in radians per second. The graph reveals chaotic behavior through its wiggling curve and the existence of subharmonics.

In the second example, the value of K was lowered to $K = 2$, and B was chosen to be 0.03, 0.08, and 0.12. The motions for $B = 0.03$ and 0.12 (Figs. 12a and 13a) are a mixture of oscillation and rotation and exhibit typical strange-attractor patterns known from the literature, with a more concentrated structure for the larger damping coefficient. Relaxing the accuracy of the Runge-Kutta scheme by an order of magnitude does not change the strange-attractor pattern. Between $B = 0.03$ and 0.12, for $B = 0.08$, the motion is non-chaotic (Fig. 14). In this picture the phase plane displays, after a transient period of irregular motion, a periodic one consisting of a combination of rotation and oscillation.

It is interesting that for moderate forcing amplitudes $(1 \leq K \leq 5)$ the strange attractor does not distinguish between the third-order (Figs. 12a, 13a) and the fifth-order (Figs. 12b, 13b, 18a, 19a) cases. The Poincaré maps are all qualitatively the same. The only difference is the tightness of the point swaths which (as is well-known) is a direct function of the total damping in the system. This result was not anticipated since these two modes are qualitatively different in their autonomous versions. The fifth-order case always has an autorotation attractor as well as a fixed point (Figs. 3 and 4), while the motion in the third-order case leads either to autorotation (Fig. 7) or to oscillation (Fig. 6) but never decays to a fixed point. The reason for the merging of these two cases in the chaotic regime should be explored in later studies.

Power spectra for the cases of Figs. 12a and 13a are displayed in Fig. 15. Again, the spectra in Fig. 15 are "continuous" with a spike at $\omega = 1$ and subharmonic values.

The influence of K was studied in a more systematic manner by increasing the values of K from 0.1 to 10 for the special force-free case shown in Fig. 4. The coefficients are $A = 0.2$, $B = -0.12$, $C = 0.01$, $D = 2$.

The phase plane for $K = 0.1$ in Fig. 16 is very similar to that for $K = 0$ in Fig. 4. The oval separatrix and open limit cycle, however, are not lines that are independent of the initial conditions but "sheets," with time as an additional coordinate. The solid and dotted lines in Fig. 16 are thus lines which do not necessarily coincide for different initial conditions. The attractors are either quasi-periodic autorotation or a fixed point.

For $K = 1$ the situation changes. After a transient time of chaos, shown on the Poincaré map in Fig. 17a as dots, the motion becomes periodic, indicated in the phase plane as a closed curve. This curve is superposed on Fig. 17a, and the corresponding Poincaré data for the closed curve are marked by a box and an arrow. The corresponding power spectrum is displayed in Fig. 17b.

6

Poincaré maps and power spectra for the cases $K = 1.5$ and 2 are shown in Figs. 18 and 19. They clearly reveal chaotic behavior.

Finally, with further increase of K to 5, the oscillatory mode dominates, and the motion becomes periodic again (Fig. 20).

By changing D from 2 to 0.2 one observes, although not shown in this report, for $K = 0.1$ a situation similar to that in Fig. 3 with a sinusoidal separatrix and attractors of either closed-limit cycle or fixed-point type. The motion exhibits autorotation for $K = 2$ and self-sustained oscillation for $K = 5$ through 10.

It is planned to obtain more physical insight into the characteristics of the strange attractors and into the frequency-coupling behavior of Eq. (3) by means of higher-order spectral analysis[12] in future studies.

ACKNOWLEDGMENT

THIS PAGE INTENTIONALLY LEFT BLANK

REFERENCES

1. Thompson, J.M.T. and H.B. Stewart, "Nonlinear Dynamics and Chaos," John Wiley & Sons, New York (1986).

2. Moon, F.C., "Chaotic Vibrations," John Wiley & Sons, New York (1987).

3. Schuster, H.G., "Deterministic Chaos," Physik-Verlag, Weinheim, FRG (1984).

4. Cox, G.G. and A.R. Lloyd, "Hydrodynamic Design Basis for Navy Ship Roll Motion Stabilization," SNAME Trans., Vol. 85, p. 51 (1977).

5. Dalzell, J.F., "An Investigation of the Applicability of the Third Degree Functional Polynomial Model to Nonlinear Ship Motion Problems," Davidson Laboratory, SIT-DL-82-9-2275 (Dec 1982).

6. Sharma, S.D., T. Jiang, and T.E. Schellin, "Dynamic Instability and Chaotic Motions of a Single-Point-Moored Tanker," 17th ONR Symposium on Naval Hydrodynamics, The Hague (1988).

7. Lamb, H., "Hydrodynamics," Sixth ed., Dover, New York, p. 174 (1945).

8. Lugt, H.J., "Autorotation," Ann. Rev. Fluid Mech., Vol. 15, p. 123 (1983).

9. Lugt, H.J., "Analogies between oscillation and rotation of bodies induced or influenced by vortex shedding," In: Vortex Motion, eds. H.G. Hornung and E.-A. Müller, Vieweg, Braunschweig, p. 82 (1982).

10. Minorsky, N., "Nonlinear Oscillations," Van Nostrand, Princeton (1962).

11. Hao, B.-L., "Chaos," 2nd reprint, World Scient. Publ., Singapore (1989).

12. Pezeshki, C. and E.H. Dowell, "On Chaos and Fractal Behavior in a Generalized Duffing's System," Physica D, Vol. 32, p. 194 (1985).

13. Gwinn, E.G. and R.M. Westervelt, "Intermittent Chaos and Low-Frequency Noise in the Driven Damped Pendulum," Phys. Rev. Lett., Vol. 54, p. 1613 (1985).

14. Grebogi, C., E. Ott, and J.A. Yorke, "Metamorphoses of Basin Boundaries in Nonlinear Dynamical Systems," Phys. Rev. Lett., Vol. 56, p. 1011 (1986).
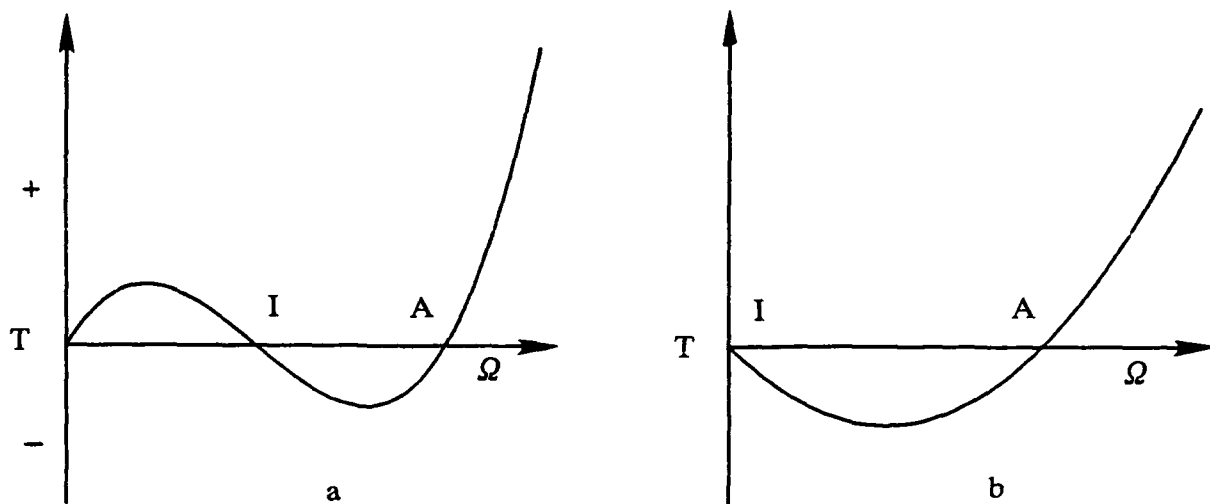
Fig. 1. Riabouchinsky curves of (a) the fifth-order type and (b) the third-order type.
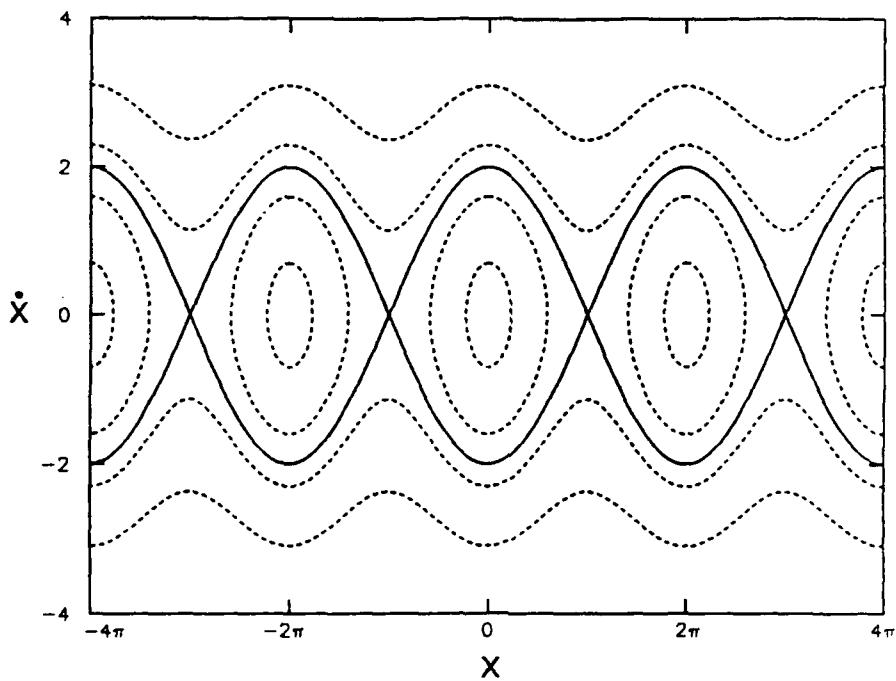
Fig. 2. Phase plane for the simple pendulum equation (1) with $D = 1$.
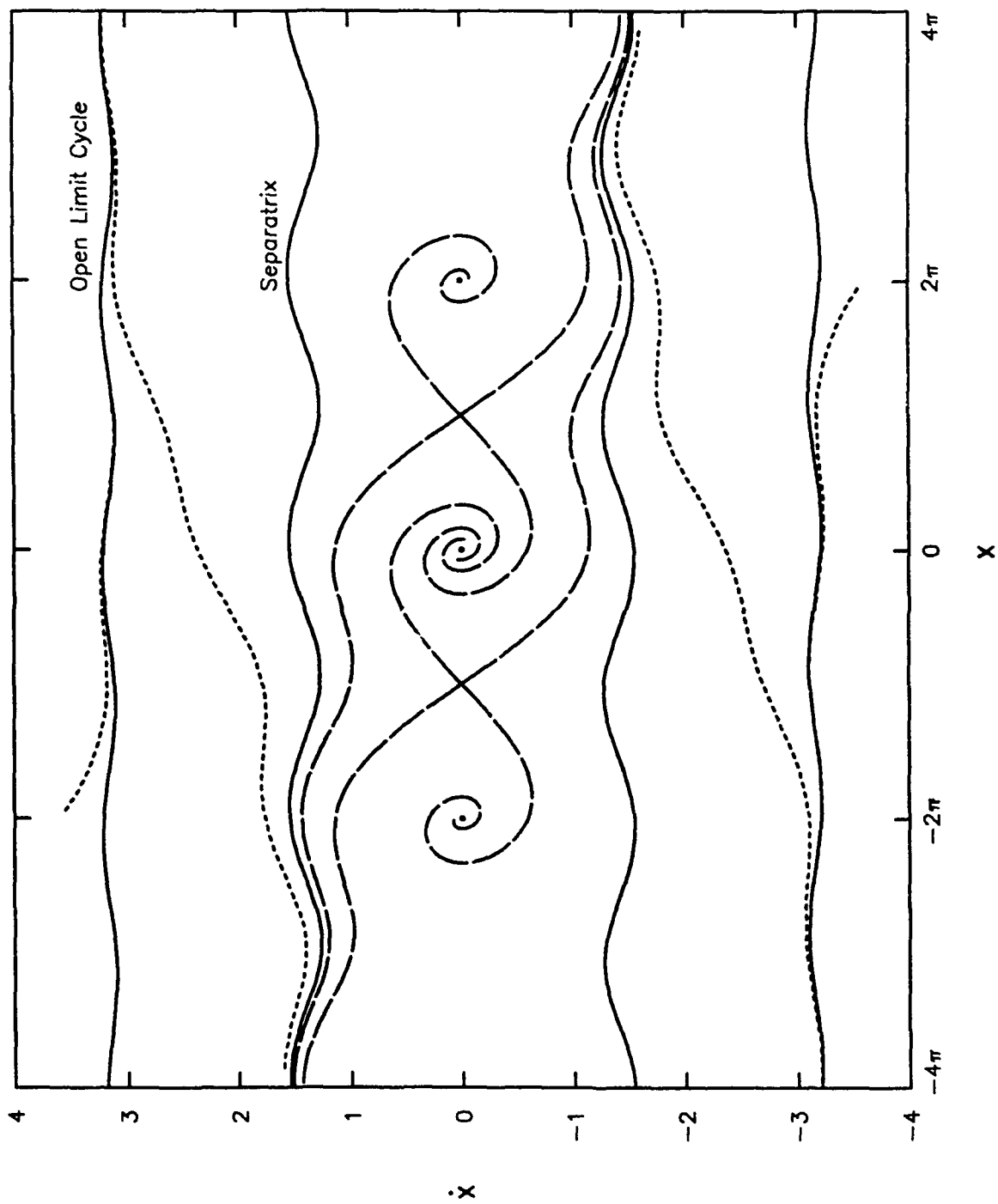
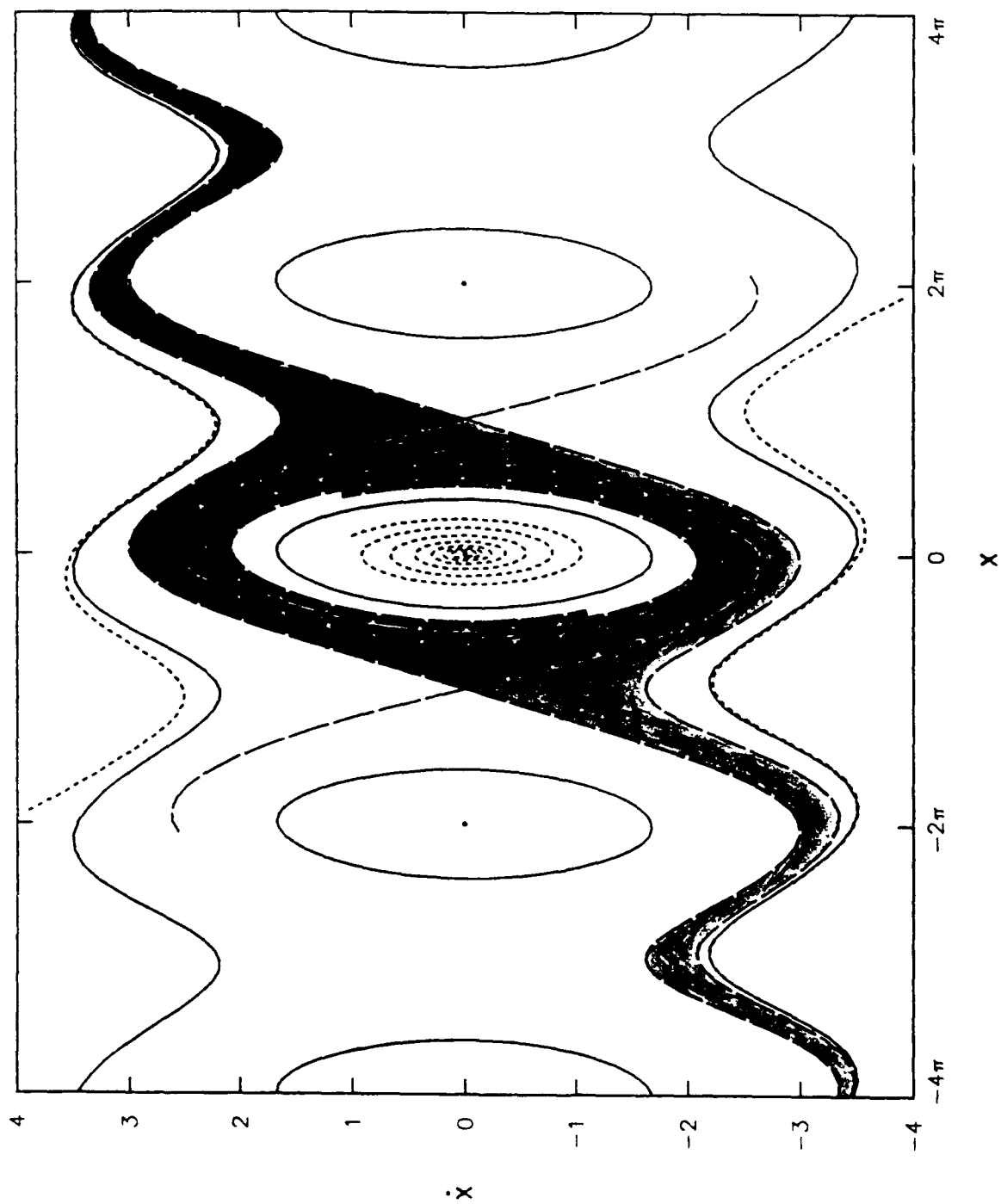**Fig. 3.** Phase plane for Eq. (2) with $A = 0.2$, $B = -0.12$, $C = 0.01$, $D = 0.2$ with a sinusoidal separatrix.

11

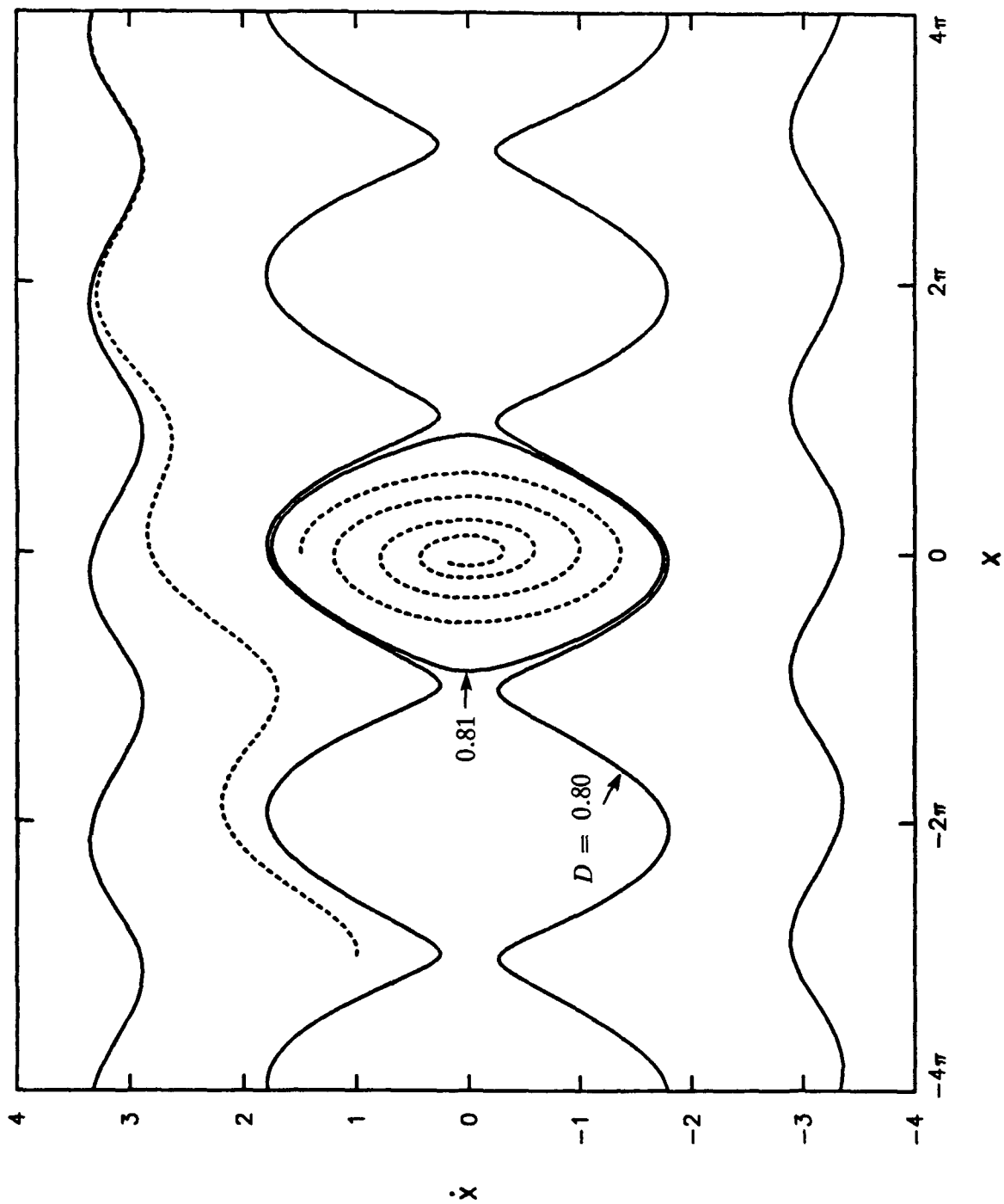**Fig. 4.** Phase plane for Eq. (2) with $A = 0.2$, $B = -0.12$, $C = 0.01$, $D = 2$ with an oval separatrix.

12

Fig. 5. Phase plane for Eq. (2) with $A = 0.2$, $B = -0.12$, $C = 0.01$, $D = 0.80$ and 0.81. Limiting case for which sinusoidal and oval separatrices collapse.

13
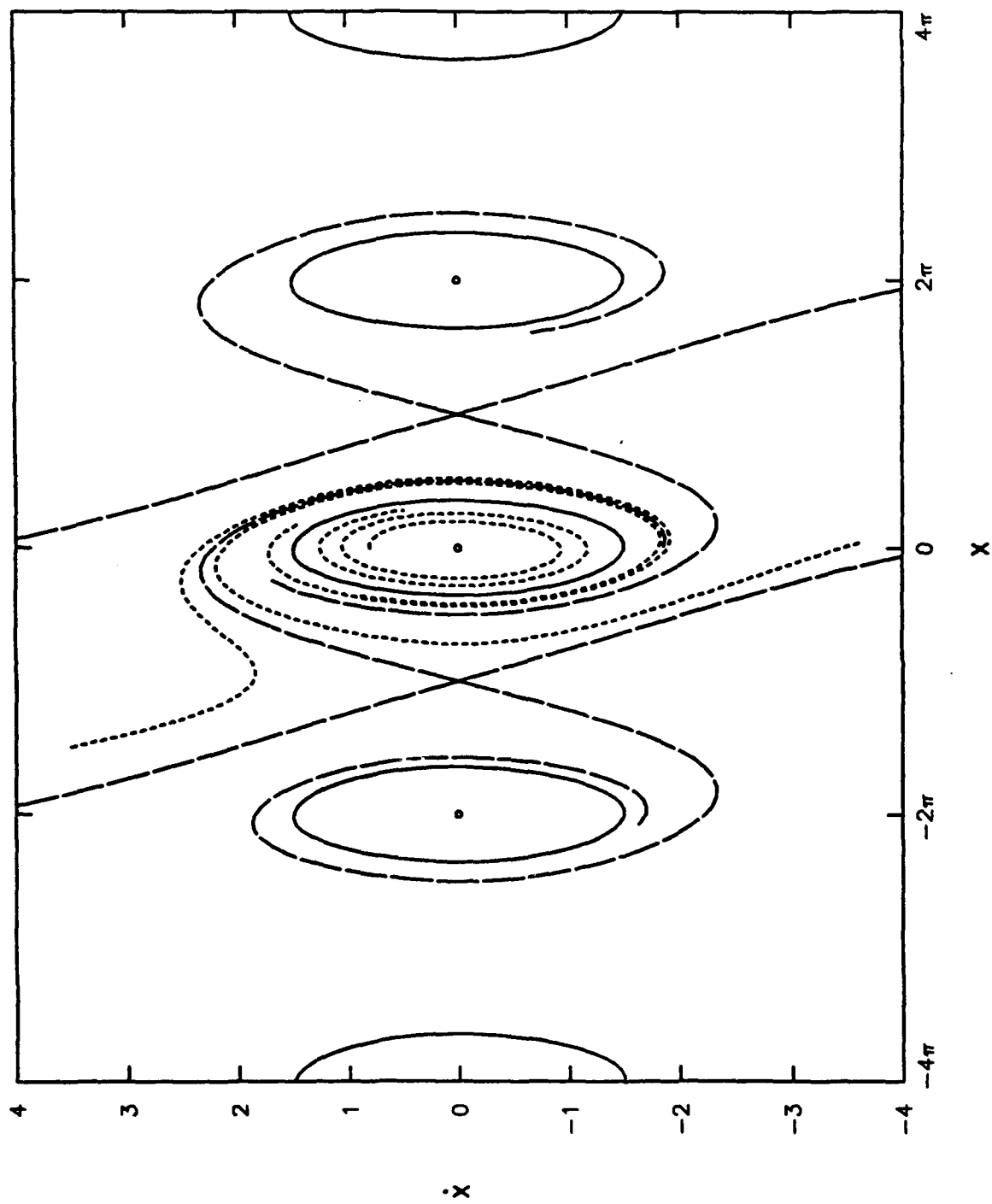
Fig. 6. Phase plane for Eq. (2) with $A = -0.2$, $B = 0.12$, $C = 0$, $D = 2$ with closed limit cycle.

14
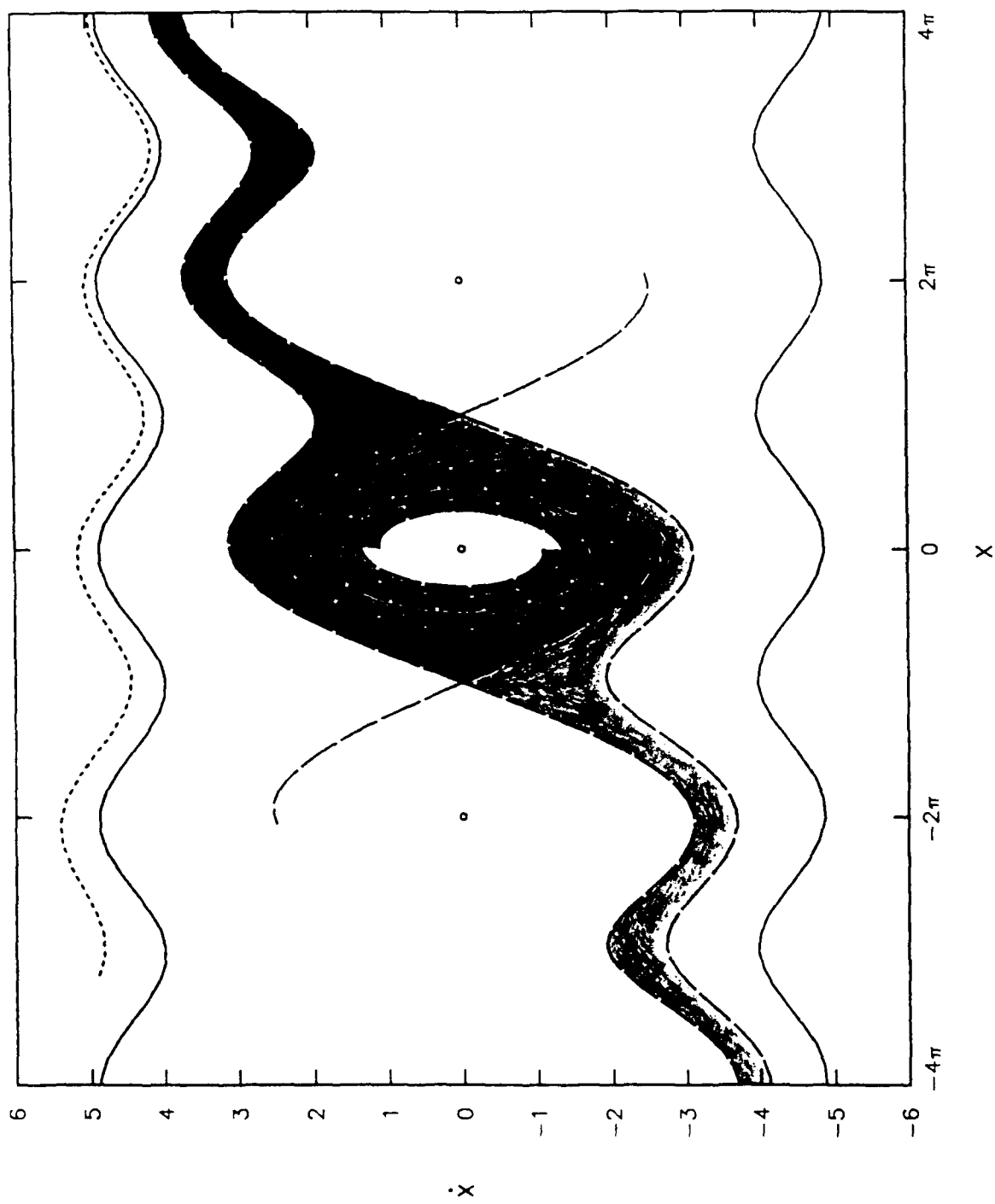
Fig. 7. Phase plane for Eq. (2) with $A = -0.2$, $B = 0.01$, $C = 0$, $D = 2$ with open limit cycle.

15
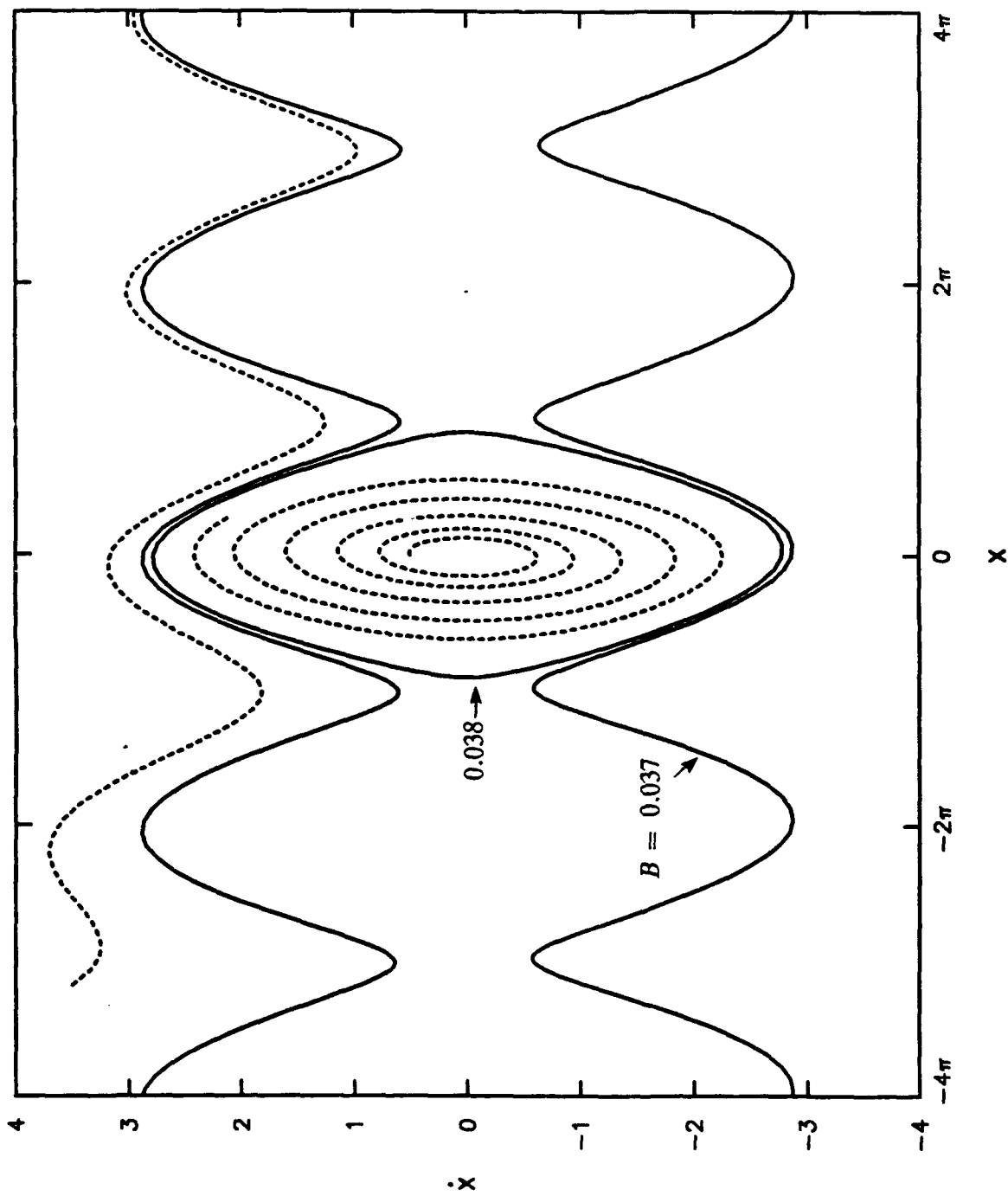
Fig. 8. Phase plane for Eq. (2) with $A = -0.2$, $B = 0.037$ and 0.038, $C = 0$, $D = 2$. Limiting case for which open and closed limit cycles collapse.
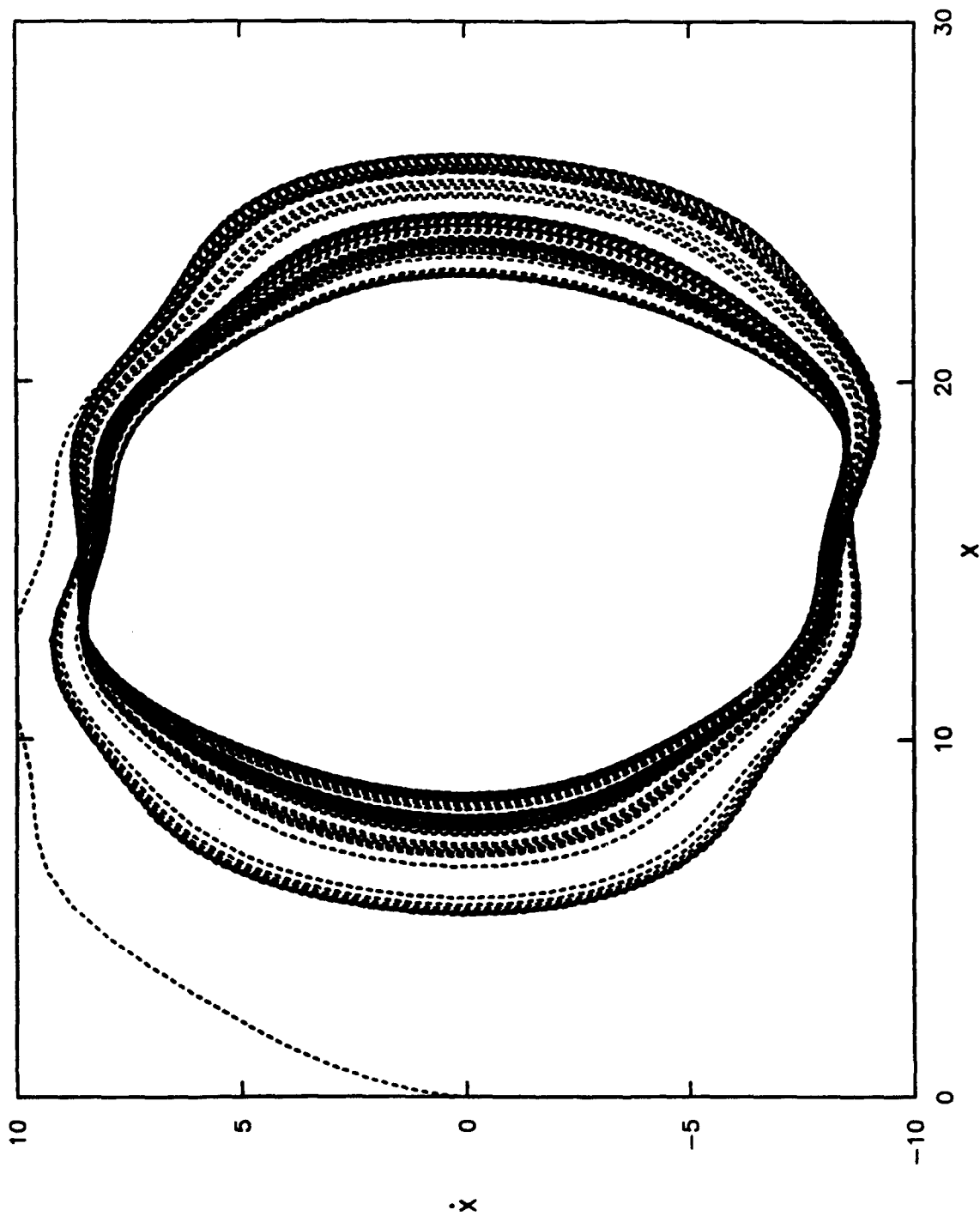
Fig. 9. Phase plane for Eq. (3) with $A = -0.2$, $B = 0.01$, $C = 0$, $D = 2$, $K_0 = 0$, $\omega^* = 1$, $\alpha = 0$, $K = 10$ and initial conditions $x_0 = \dot{x}_0 = 0$.
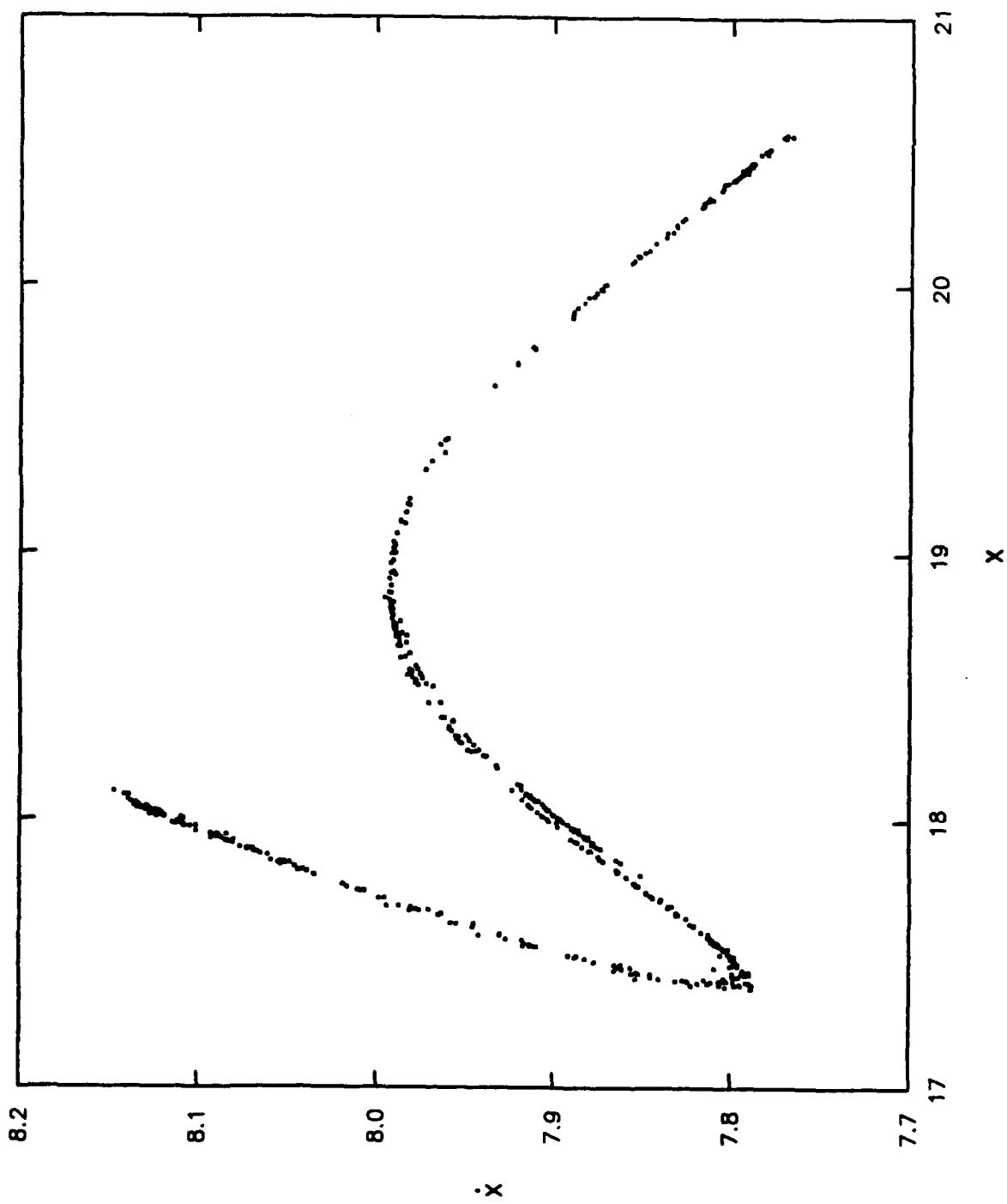
Fig. 10. Poincaré map for the case of Fig. 9.

18
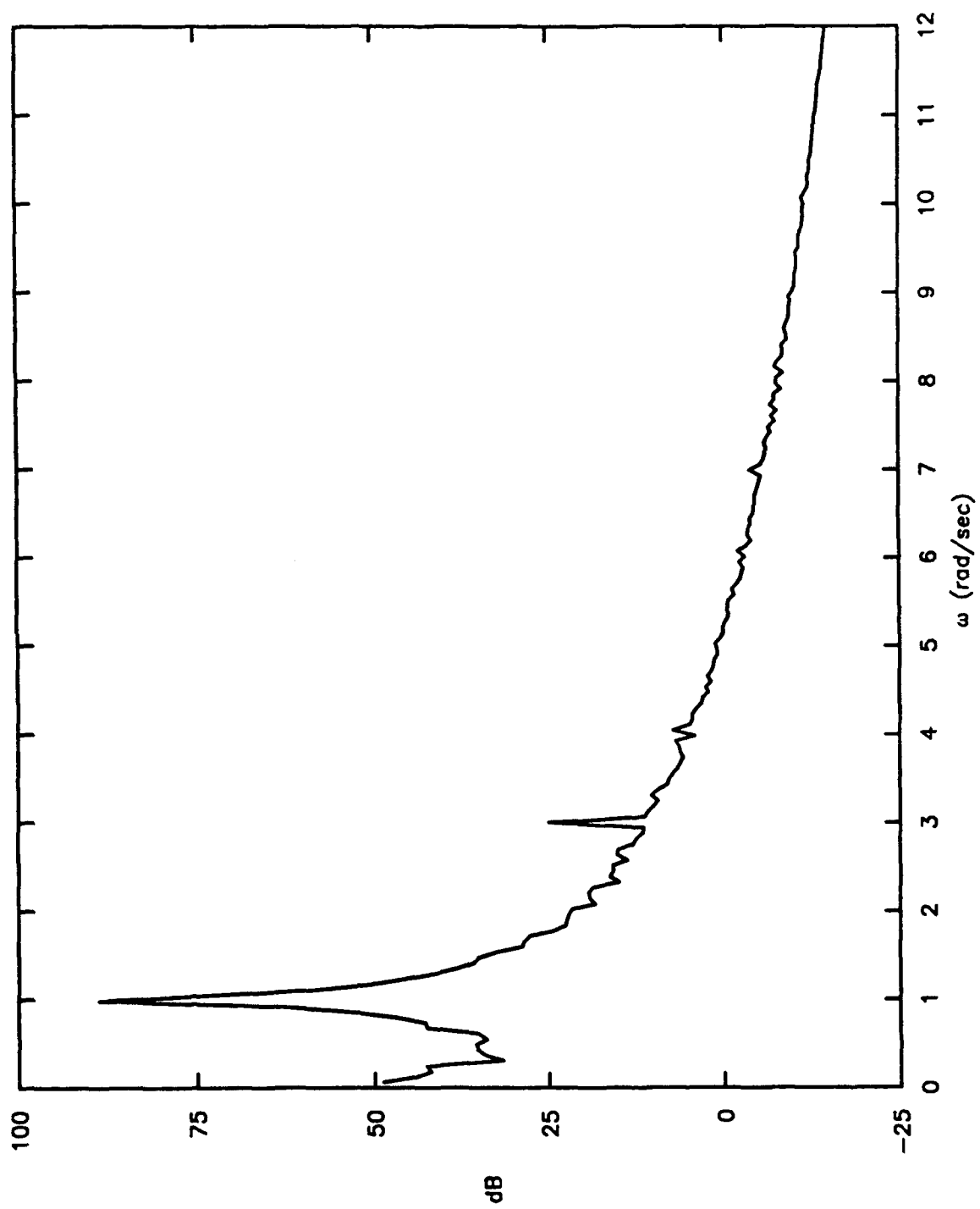
Fig. 11. Power spectrum for the case of Fig. 9.
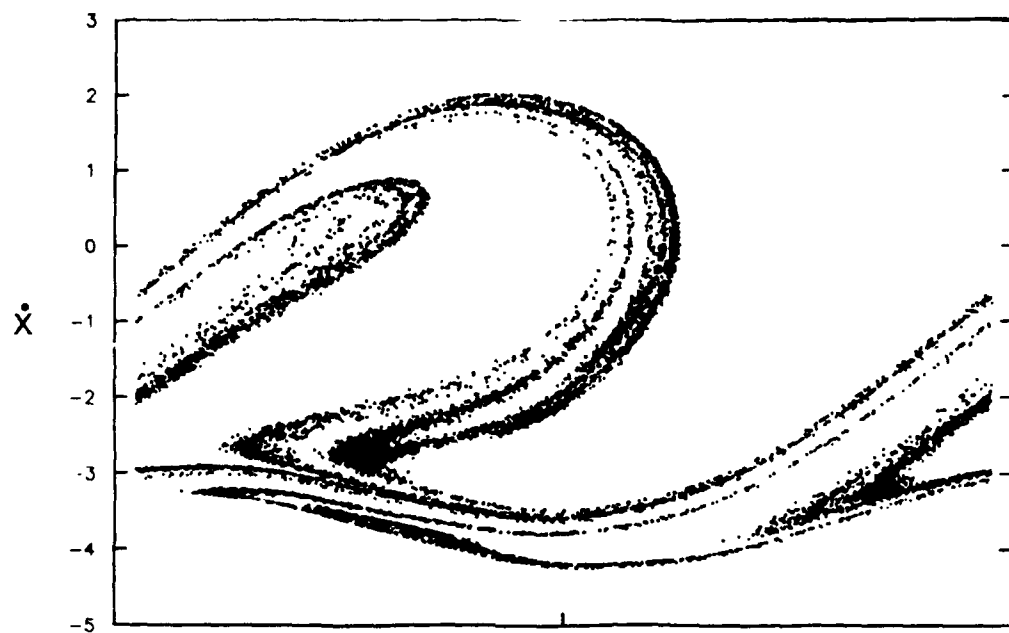
a
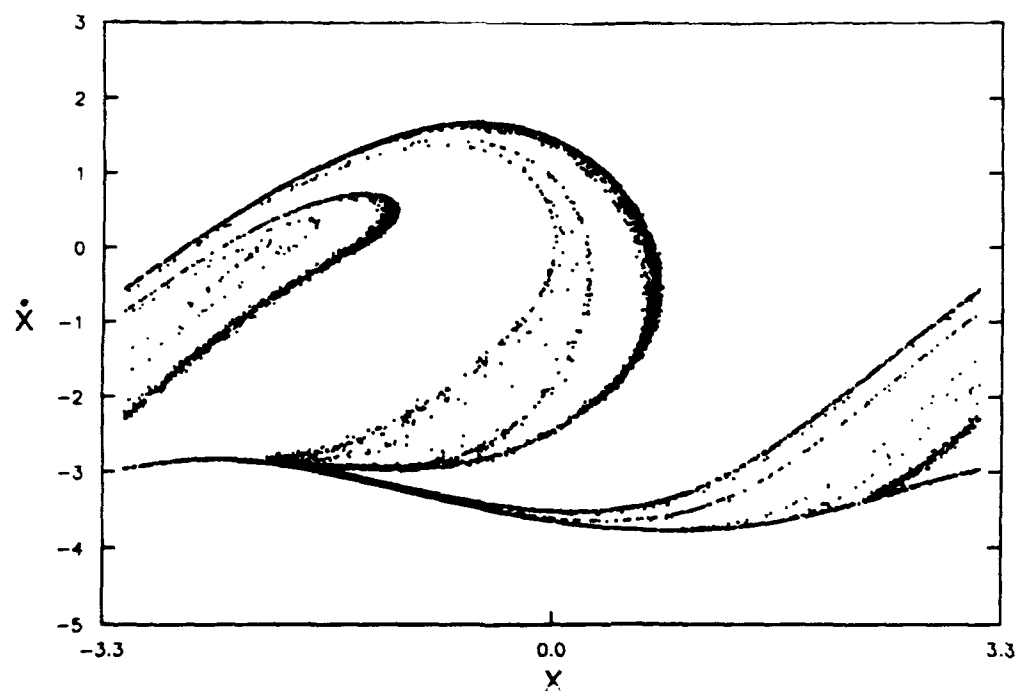
b

Fig. 12. Poincaré maps for the coefficients (a) A = −0.2, B = 0.03, C = 0, D = K − 2 and for (b) A = 0.2, B = −0.12, C = 0.01, D = K = 2.
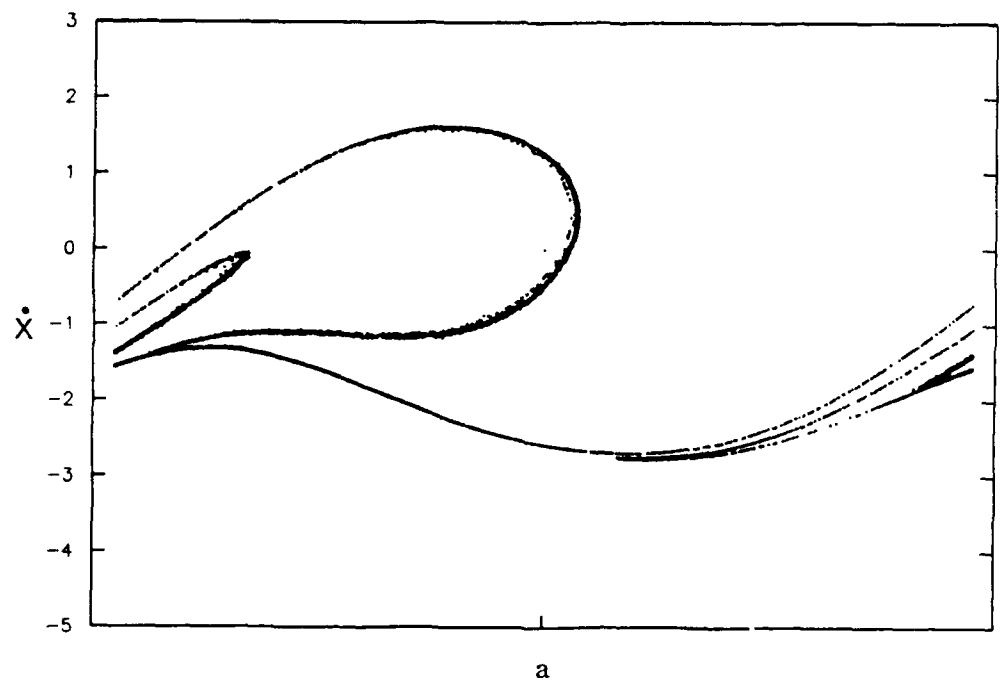
20
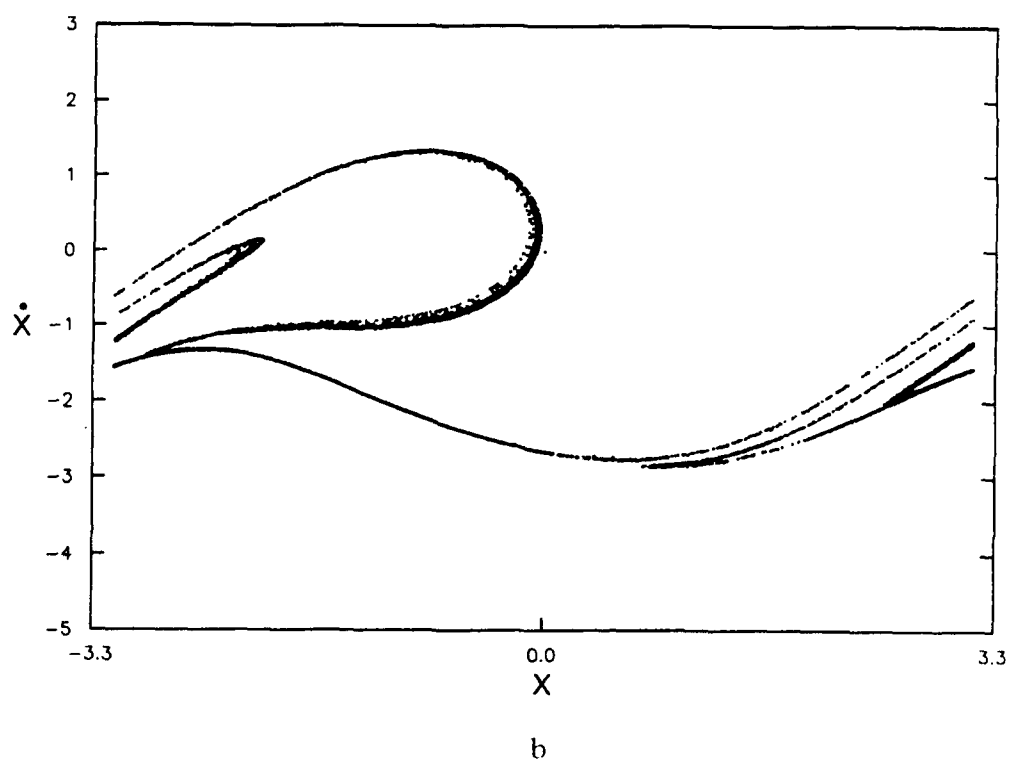
Fig. 13. Poincaré maps for the coefficients (a) A = –0.2, B = 0.12, C = 0, D = K = 2 and for (b) A = 0.2, B = –0.02, C = 0.01, D = K = 2.
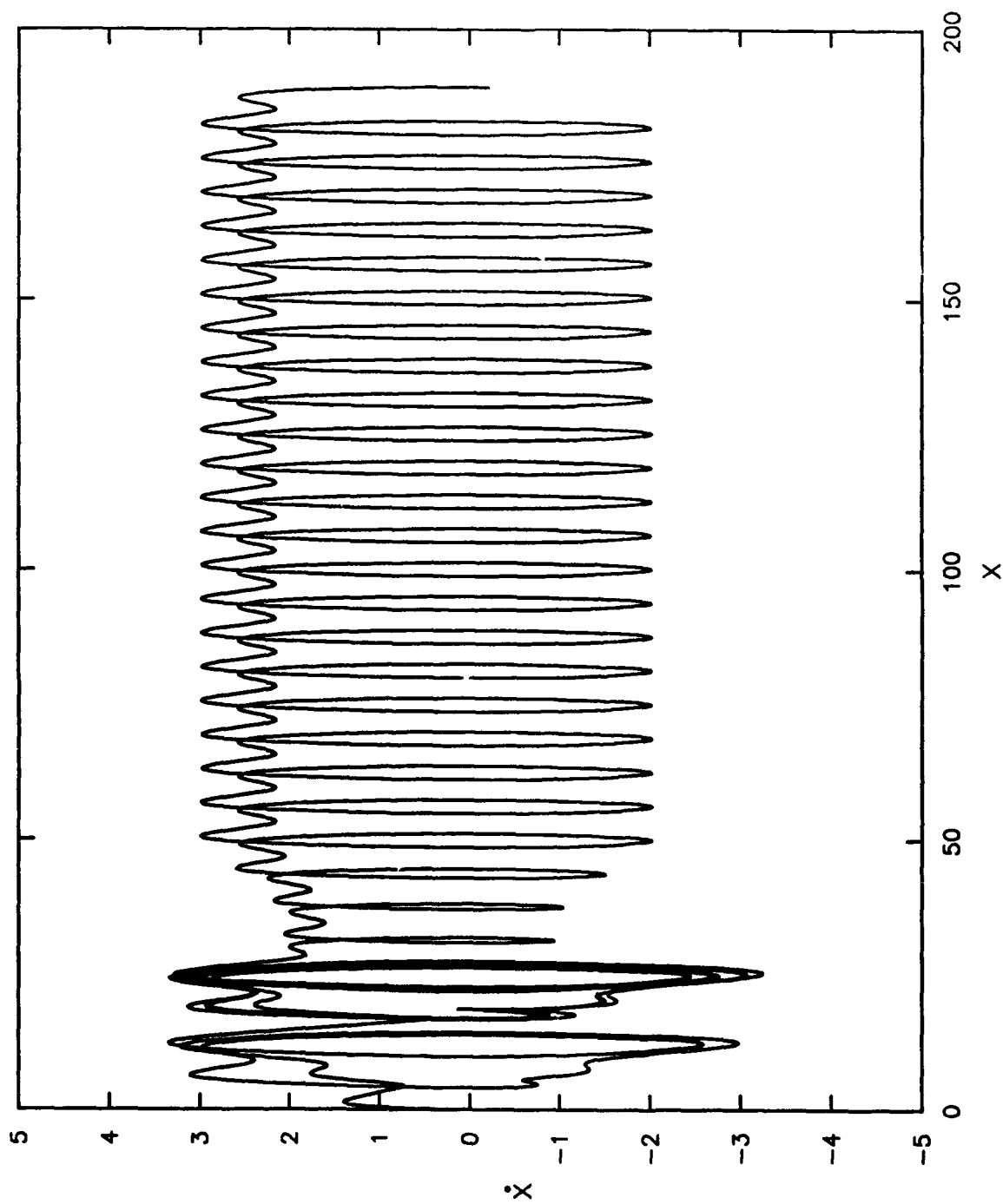
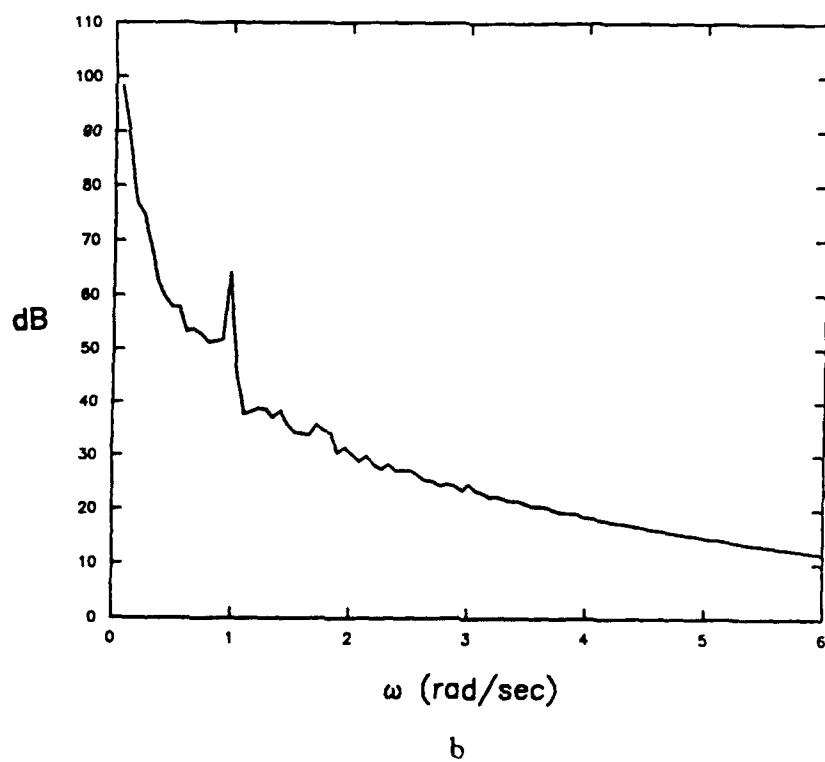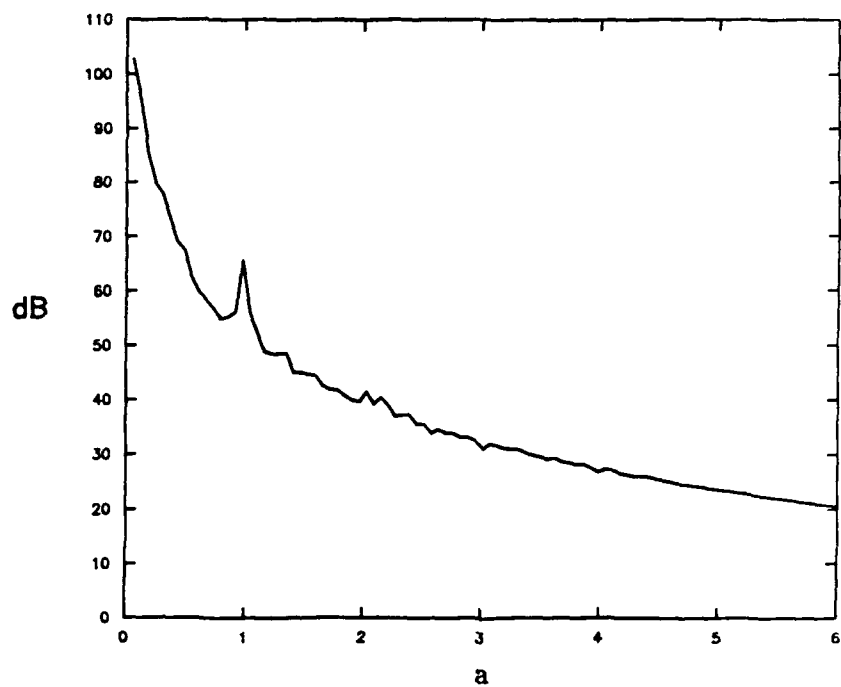**Fig. 14.** Phase plane for the case of Fig. 12a but with $\mathcal{B} = 0.08$.

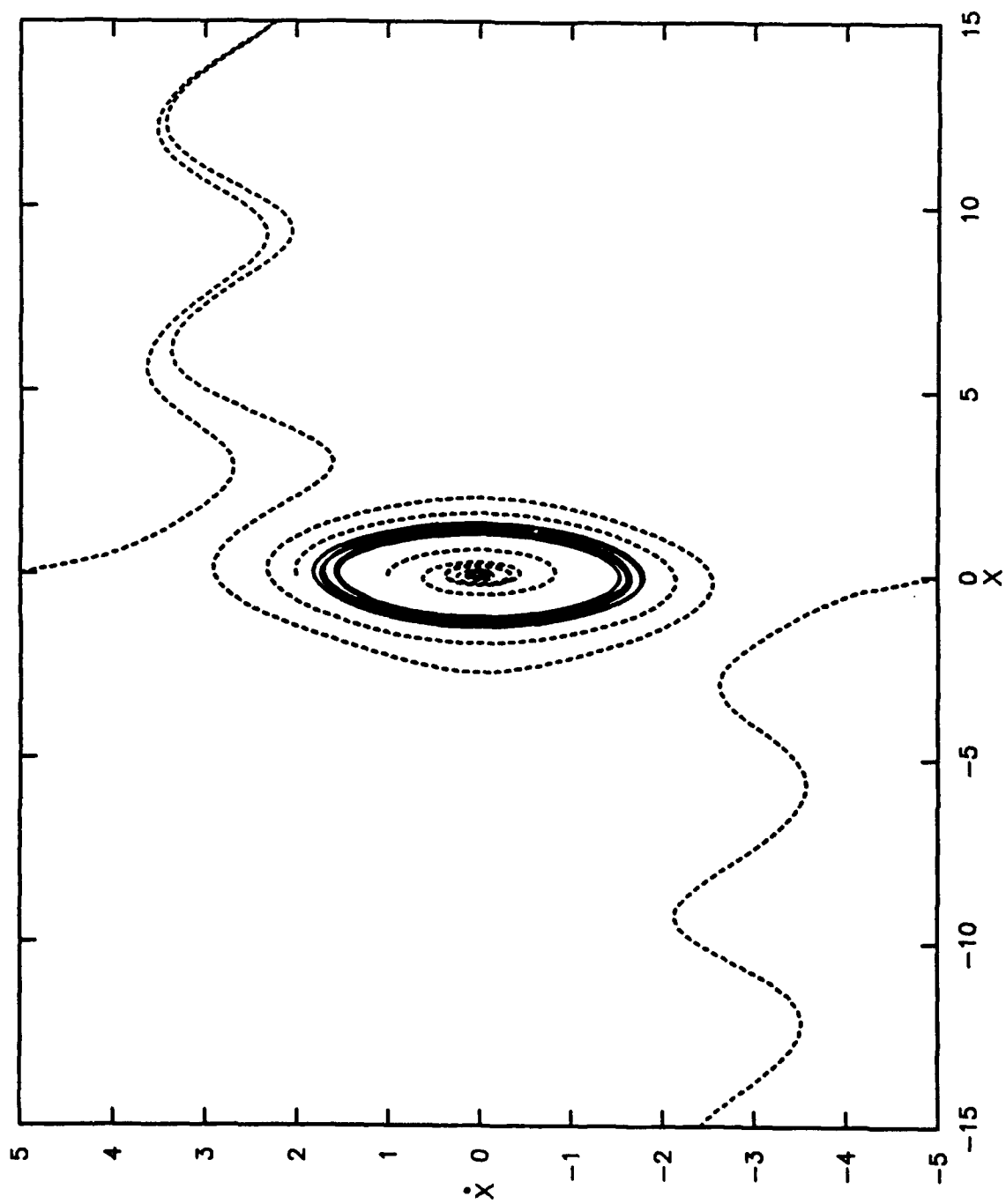**Fig. 15.** Power spectra for the two cases of Figs. 12a and 13a.

23

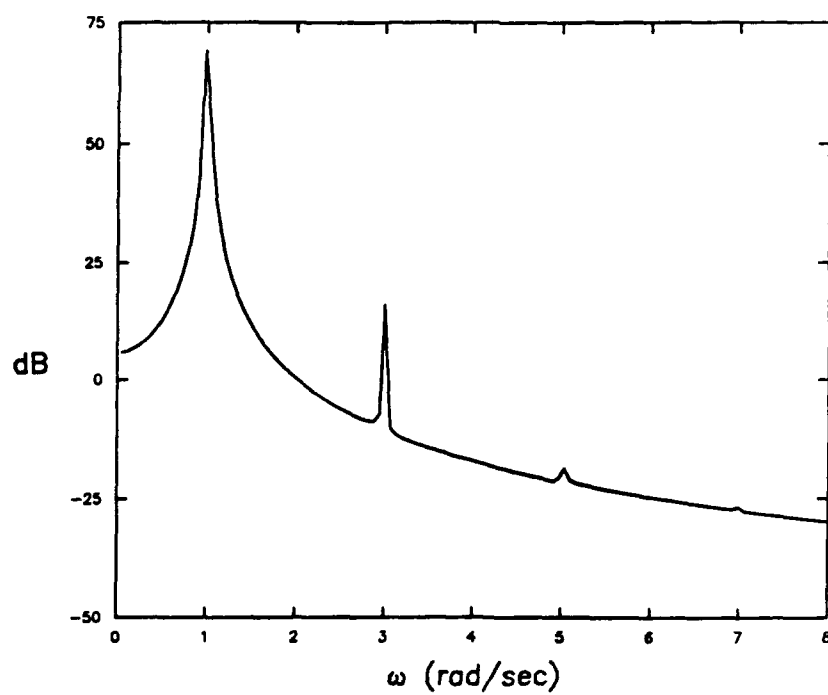**Fig. 16.** Phase plane for Eq. (3) with $A = 0.2$, $B = -0.12$, $C = 0.01$, $D = 2$, and $K = 0.1$.
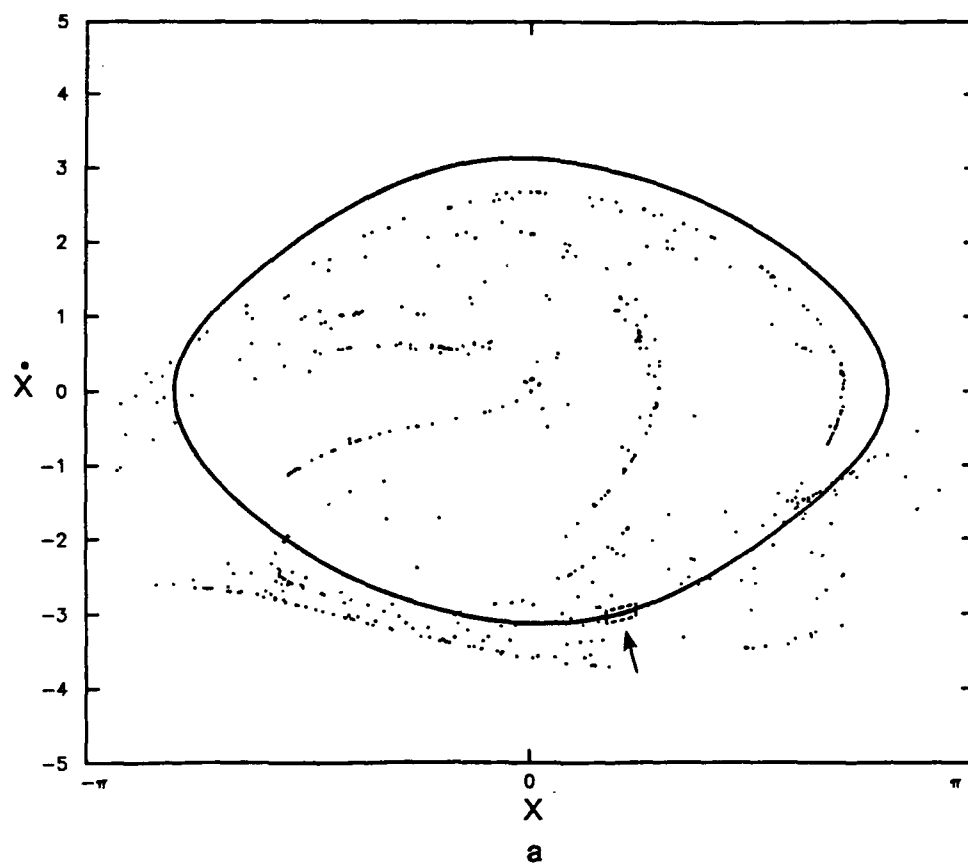
Fig. 17. Poincaré map (a) and power spectrum (b) with the same coefficients as in Fig. 16 but with $K = 1$.
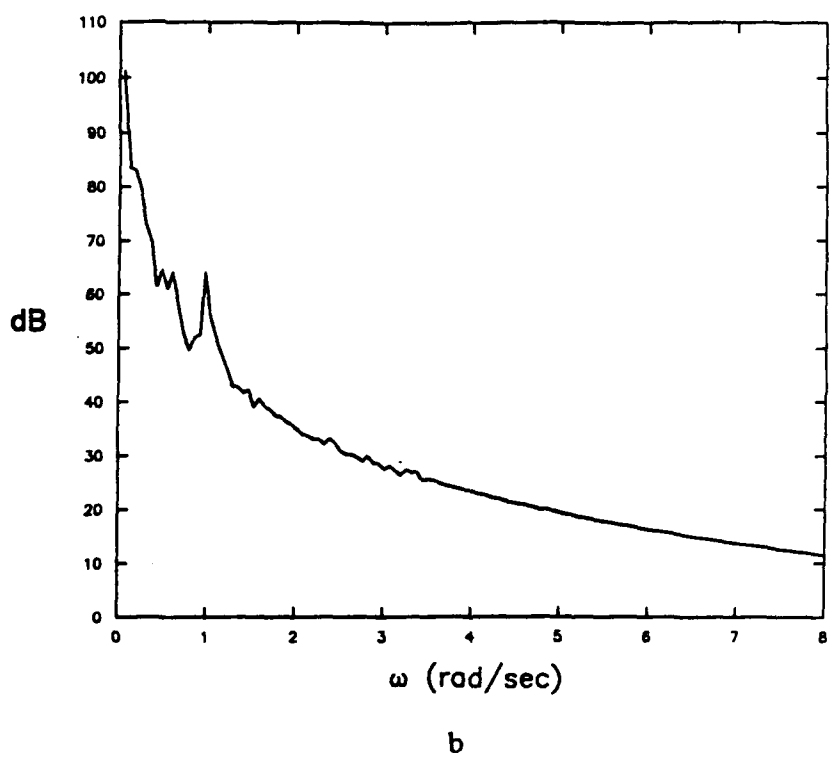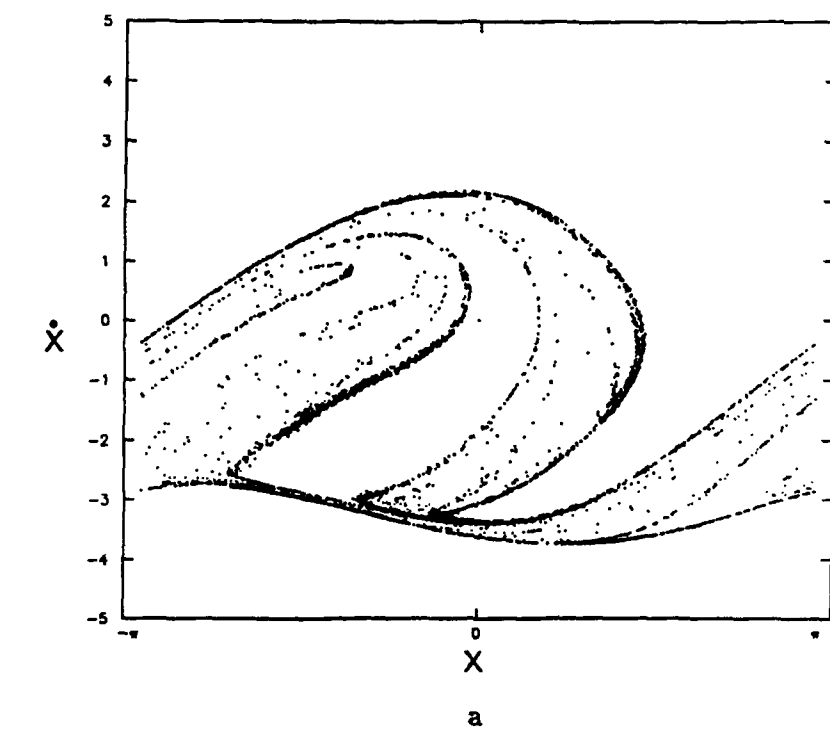
Fig. 18. Poincaré map (a) and power spectrum (b) with the same coefficients as in Fig. 16 but with $K = 1.5$.
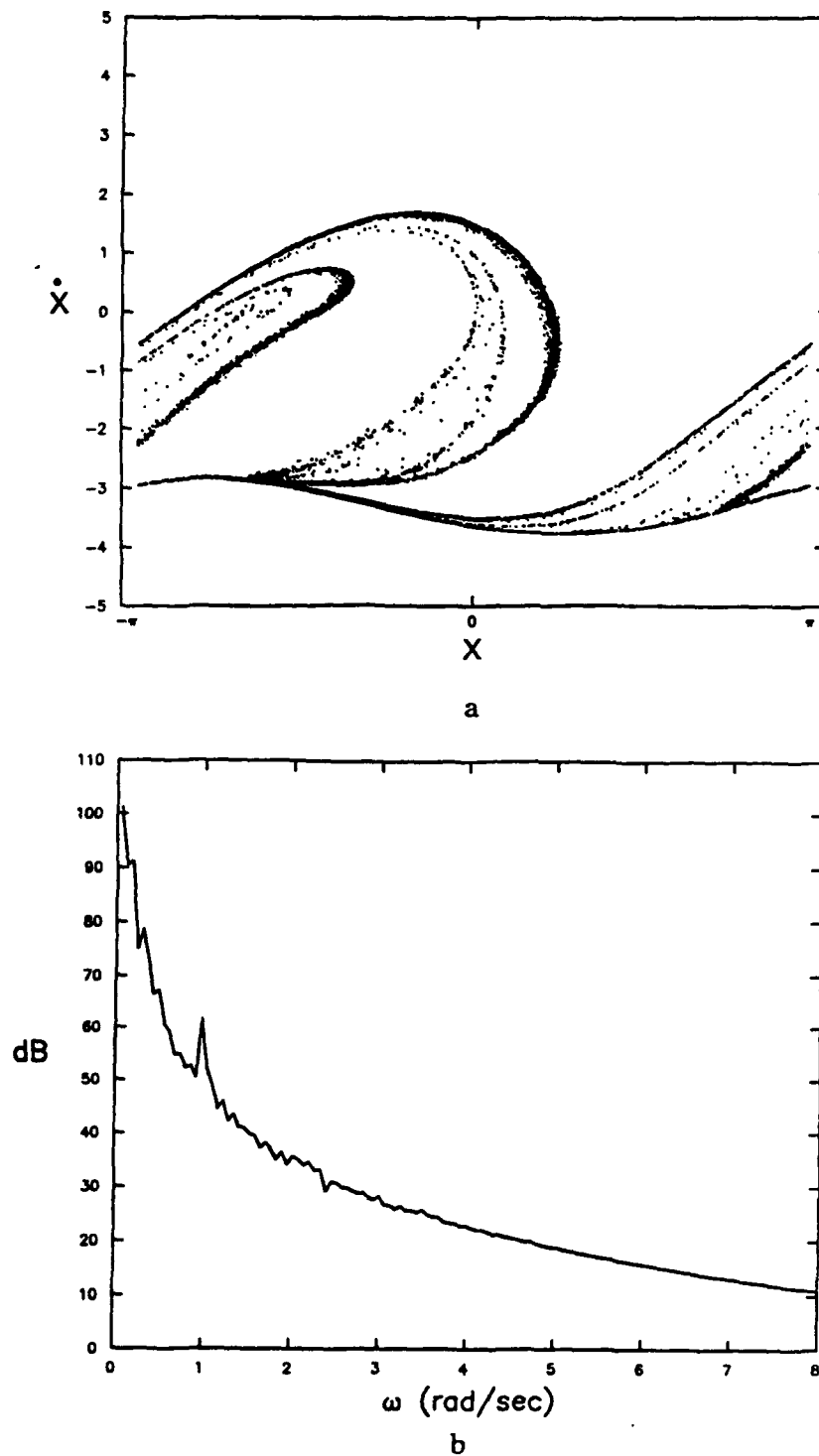
Fig. 19. Poincaré map (a) and power spectrum (b) with the same coefficients as in Fig. 16 but with $K = 2$.
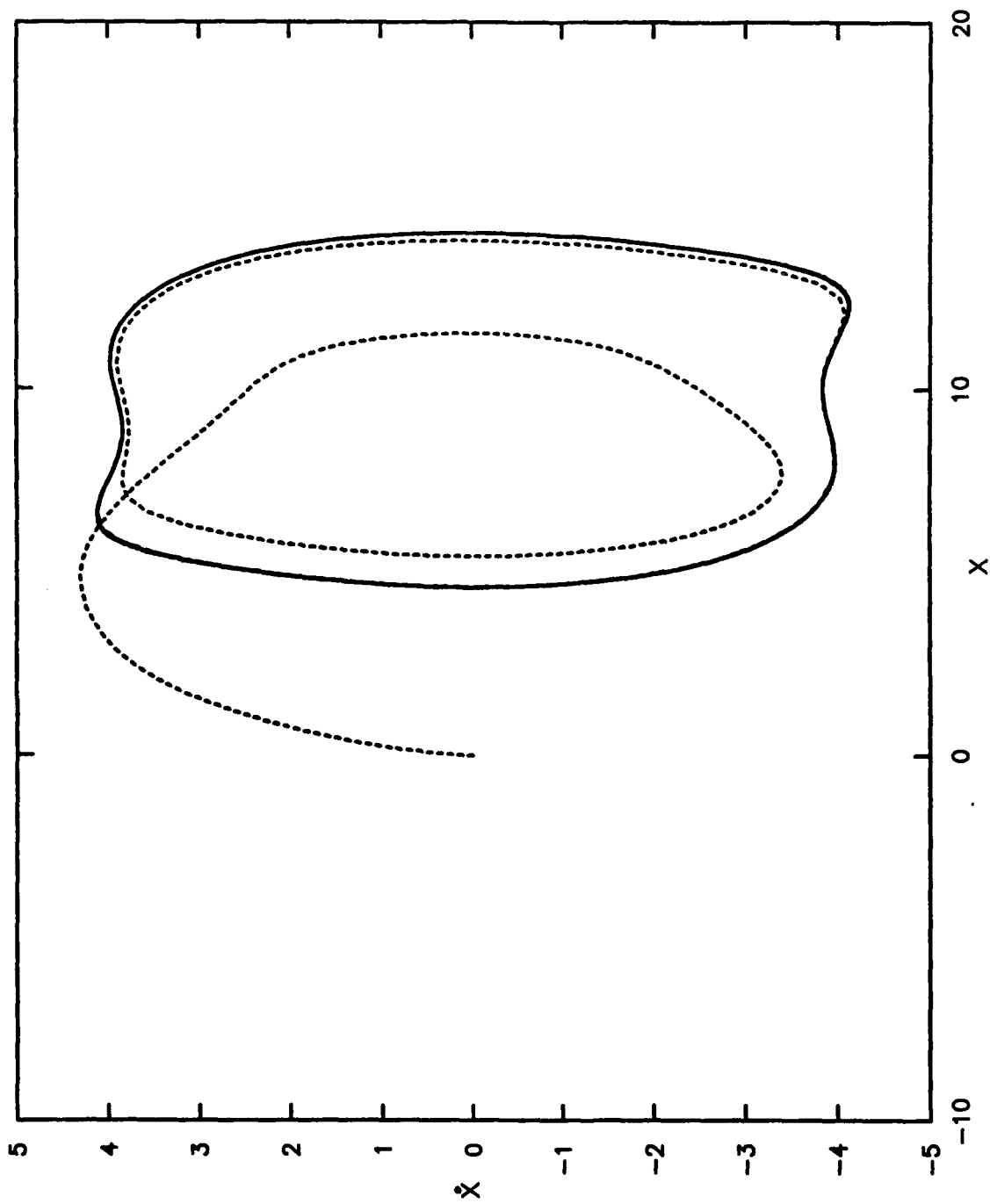
27

Fig. 20. Phase plane with the same coefficients as in Fig. 16 but with $K = 5$.

28

INITIAL DISTRIBUTION

Copies

1	DARPA
4	ONR
	1 M.M. Reischman
	1 M.F. Shlesinger
	1 E.P. Rood
	1 S.E. Ramberg
3	NAVSEA
	1 SEA 05, RADM Ricketts
	1 W. Sandberg
	1 Lib
2	USNA
	1 R.A. GRANGER
	1 Tech Lib
3	NRL
	1 Library
	1 O.M. Griffin
	1 H.T. Wang
1	NAVPGSCOL
	1 Lib
1	NSWC/Dahlgren/Lib
1	NSWC/White Oak/Lib
1	NAVSHIPENGCEN/Tech Lib
12	DTIC
1	Library Congress
	1 Science and Tech Division
1	NASA Langley Res Center/Lib
2	NASA Ames Res. Center
	1 Library
	1 B.G. McLachlan
1	NASA Lewis Res Center/Lib

Copies

1	Air Force Flight Dynamics Lab/ Lib
1	U.S. Army Ballistic Res Lab/Lib
1	NIST/Lib
2	University of California, Berkeley
	1 Library
	1 S.A. Berger
1	University of California, San Diego / Library
2	Calif Inst. of Technology
	1 Library
	1 T.Y. Wu
1	University of Iowa
	1 Library
1	Lawrence Livermore Nat Lab
	1 Library
3	University of Maryland
	1 Library
	1 J.A. Yorke
	1 C. von Kerczek
3	University of Michigan
	1 Library
	1 G. Tryggvason
	1 W.W. Willmarth
4	MIT
	1 Library
	1 J.N. Newman
	1 T.F. Ogilvie
	1 G.S. Triantafyllou

INITIAL DISTRIBUTION (Continued)

1   Washington State University

      1   C. Pezeshki

CENTER DISTRIBUTION

Copies	Code	Name
1	00	C. Graham
1	01	R. Metrey
1	01A	D.J. Sheridan
1	011	E. O'Neill
5	0113	B.E. Douglas
1	0117	B. Nakonechny
1	0118	D.D. Moran
1	12	G.D. Kerr
1	15	W.B. Morgan

Copies	Code	Name
1	1501	H.J. Haussling
1	154	J.H. McCarthy
1	1542	T.T. Huang
1	1543	L.P. Purtell
1	1544	F.B. Peterson
1	1544	A.M. Reed
1	156	D.S. Cieslowski
20	1802	H.J. Lugt
1	184	M. Hurwitz
1	1843	R.T. Van Eseltine
20	1843	M. Brabanski
1	342.1	TIC (C)
1	342.2	TIC (A)
10	3432	Reports Control